Measurements of dc SQUID damping effects on superconducting resonant circuits

E. C. van Assendelft, H.-M. Cho, J. Corbin, S. Kuentsner, D. Li,

A. Phipps, N. Rapidis, J. Singh, K. Wells, K. D. Irwin

***Abstract*—We present experimental measurements of SQUID-induced damping effects on strongly coupled, lumped-element resonators in the 500kHz-1MHz frequency range. While dc SQUIDs are commonly used for sensitive readout of electromagnetic signals such as in lumped-element axion dark matter searches, coupling a dc SQUID to a resonant circuit modifies the circuit's resonance frequency, quality factor, noise, and impedance. These parameters have a direct impact on the science reach of axion dark matter detectors, making it important to understand SQUID damping contributions. We describe a helium dip probe and two-stage SQUID readout scheme used to probe SQUID damping effects. Measurements from this setup inform the design and operation of both future test platforms as well as next-generation dark-matter experiments.**

***Index Terms*—SQUIDs, circuits, superconducting resonators**

I. Introduction

The high bandwidth and dynamic range, low noise characteristics, and maturity of dc superconducting quantum interference devices (dc SQUIDs) make them a versatile tool for a variety of precision measurements, including readout of resonant circuits in applications such as quantum information, dark matter detection, and gravitational wave detection. However, the dc SQUID is a lossy active circuit with a dynamic input impedance that varies based on its detailed design and operating point, and the SQUID's dynamic input impedance modifies the resonance frequency, quality factor, noise, and impedance of a resonant circuit [1]. Understanding SQUID damping as a function of operating parameters is essential to optimize dc SQUID readout systems used in precision experiments.

Axion and hidden-photon detectors are an important application where dc SQUIDs have become a standard measurement tool [2]–[9]. Axions, a leading dark-matter candidate, are low mass particles that behave as a classical wave. In the presence of a magnetic field, axion-photon coupling produces an effective axion current oscillating at a frequency set by the axion mass. The expected signal strength is small, so axion dark matter experiments use resonant pickup structures with high quality factor Q to improve the impedance match to the dark matter signal [10]. At frequencies in the kHz-MHz range (corresponding to axion masses of peV to $\mu\mathrm{eV}$), lumped element resonators are used to implement detectors with a wide tuning range. The science reach of resonant axionic dark matter searches are determined by the rate at which they can scan through frequencies at a desired sensitivity. The resonator frequency can be impacted by SQUID effects. Additionally, the scan rate of the experiment is directly proportional to the quality factor of the resonant pickup structure, which is affected by SQUID damping contributions [11].

SQUID damping contributions depend on the detailed device design and operating parameters, so it is useful to create a test platform to investigate dc SQUID devices and readout configurations. We investigate SQUID effects in a low-Q, high coupling regime, but these results are applicable to the high-Q, low coupling regime that is relevant for future axion dark matter detectors such as DMRadio-m^3.

II. Experimental setup

To directly characterize damping in the strongly coupled, low-Q resonator regime, a dip probe is the natural solution. The liquid helium dip probe, shown in Figure 2, provides fast thermal cycling. In addition, the wiring of the 4K readout PCB and room temperature control electronics enable flexible measurement capabilities and in-situ control over many SQUID operational parameters.

The readout circuit consists of a two-stage SQUID arrangement and is illustrated in Figure 1. The two dc SQUID chips are identical Time Division Multiplexing (TDM) chips fabricated at NIST [12]. Each chip is made up of 11 channels of SQUID arrays, each array consisting of four SQUIDs in series, selectively activated via Zappe interferometers that act as switches. The Zappe interferometers consist of three junctions in parallel with two loops [13]. The supercurrent of the Zappe interferometer is modulated between zero and the junctions' critical current by applying magnetic flux. When the supercurrent is tuned to zero current, the switch acts as a resistive "open" and the SQUID channel can be biased. When the switch is "off," the Zappe interferometer acts as a superconducting short around the SQUID channel, turning the SQUID off. Multiple channels can be turned on simultaneously, which combines their outputs in series. The capability to change the number of SQUIDs in series that are turned on while cold makes these chips ideal for characterizing the facility with different impedances.

The SQUID chip has a feedback coil that is common to all SQUID channels, and is used to apply flux bias signals or feedback when operating in a flux-locked-loop (FLL) mode. The first-stage SQUID channels are voltage-biased using a 3Ω resistor, and the output is connected in series with the input coil of the second-stage SQUID chip. The second-stage SQUID, which is current biased, amplifies the response of the first-stage SQUID chip. SQUID biases, feedback signals, flux offsets, and voltage readout of the second-stage SQUID output are provided by Magnicon XXF1 electronics [14].

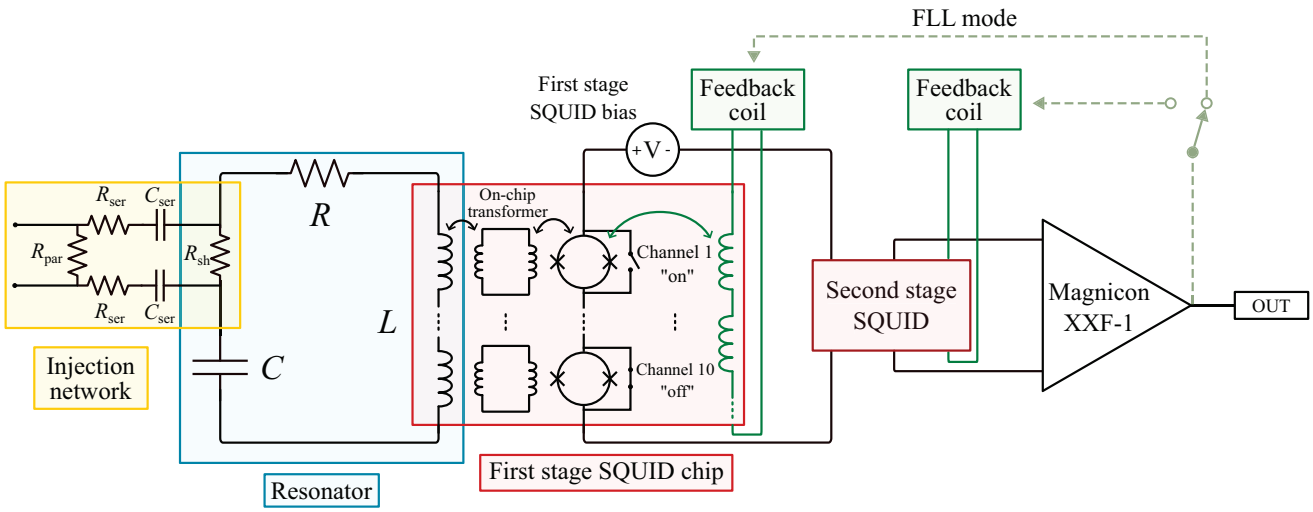

Fig. 1. Wiring diagram of dip probe circuit. The first-stage SQUID chip consists of multiple channels of SQUID arrays wired in series. Each SQUID channel (up to ten) can be individually turned on using Zappe interferometer "switches". When the switches are in the "off" position, the SQUID channel is shorted. All SQUID channels are addressable via a common feedback coil coupled inductively to the SQUID loops. Each SQUID channel is inductively coupled via an on-chip transformer to the input coil. A resonant circuit is created by adding capacitance across the first-stage SQUID input coil. For the following measurements, two configurations were used: a single niobium foil and teflon dielectric capacitor, or two NPO capacitors wired in parallel. Additionally, a network of resistors and capacitors allows a signal to be injected into the resonator in series with the capacitor. The output of the first-stage SQUID is amplified by a second-stage SQUID chip of the same design (details in the diagram are omitted for clarity). The output of the second-stage SQUID is amplified by Magnicon XXF-1 readout electronics at room temperature. The two-stage SQUID arrangement is operated either in open loop mode, or in flux-locked-loop mode which uses an integrator circuit to provide a signal to the feedback coil that keeps the total flux threading either the first- or second-stage SQUID constant.

The input coils for ten channels on the first-stage SQUID are wire bonded in series. The SQUID chips are wire bonded such that the switches for each channel are individually addressable from room temperature, meaning anywhere between one and all available channels (up to ten for the first-stage SQUID, and up to eight for the second-stage SQUID) can be activated simultaneously.

The first stage SQUID chip input coil is coupled to the SQUID channels with an on-chip transformer, and connected to two niobium screw terminals which provide the ability to easily change the configuration of the input circuit. Components such as a capacitor are attached to create a series resonator with the input coil inductance of the first-stage SQUID chip. To measure the transfer function of the resonator, a network of SMD resistors and capacitors is used to inject a voltage across a shunt resistor in series with the SQUID input coil. The shunt resistor is a single aluminum wirebond; its resistance is estimated from previous measurements of wirebonds with comparable dimensions. Surface mount component values, included in Table I, are chosen to create a large

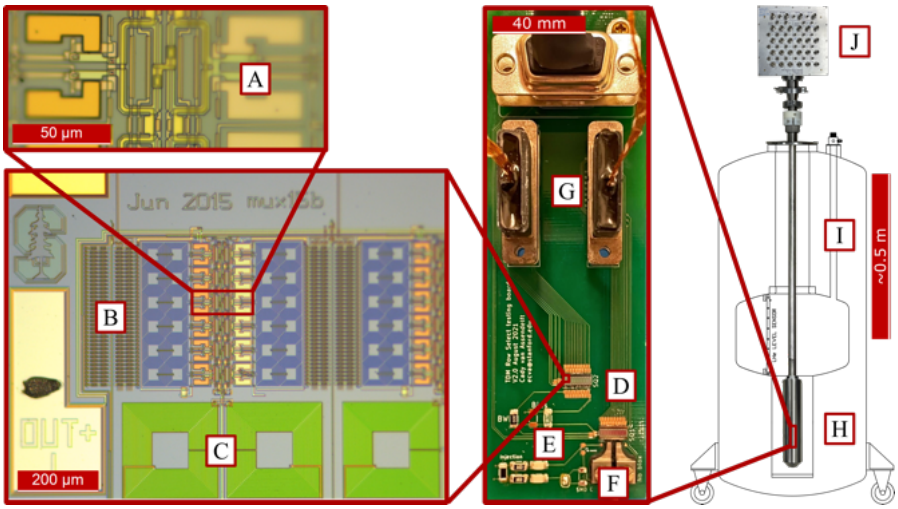

Fig. 2. Photos of the SQUID chip, readout PCB, and dip probe assembly. A) One SQUID on a NIST-fabricated TDM chip. Four SQUIDs wired in series comprise a single channel. B) Zappe interferometer switches. C) Input transformer. D) First- and second-stage SQUID chips. E) Injection network of surface mount components. F) Niobium screw terminals wirebonded to first-stage SQUID input. G) Wiring looms from 4K PCB to room temperature. H) Cryoperm shielding surrounding SQUID readout PCB. I) Liquid helium dewar cross-section. J) Room temperature breakout box.

effective resistance in parallel with the shunt wirebond so that the total resistance in the circuit is not modified by presence of the injection network. The resistor values are measured using a four-point measurement at 4K using a dip probe. The series capacitor value is the stated data sheet value at room temperature.

TABLE I
INJECTION NETWORK VALUES

Parameter	Value	Description
R_{sh}	1-5 mΩ	one wirebond (estimated)
R_{par}	$499.851 \pm 0.0011\Omega$	thin-film resistor (measured)
R_{ser}	$10.018 \pm 0.002\text{k}\Omega$	thin-film resistors (measured)
C_{ser}	1 nF	NPO capacitors (datasheet value)

The SQUID readout PCB and capacitor are enclosed in a high permeability Cryoperm cylinder to provide magnetic shielding [15]. The shielding factor for the Cryoperm was measured to be 715 at room temperature using a Bartington Mag 649 magnetic field sensor, which has a bandwidth of 1kHz. Wiring looms connect the SQUID PCB to a room-temperature breakout box, where signals are injected or read out. Physical switches on the breakout box allow signals such as the feedback/flux offset signals and SQUID bias values to be sourced from the Magnicon XXF1 electronics or directly from signal generators. The SQUIDs can also be operated in flux-locked-loop (FLL) mode to increase the bandwidth and linearity. The FLL mode uses an integrator circuit, which provides a signal via the feedback coil that keeps the first-stage SQUID operating point constant. An image of the dip probe and SQUID readout circuit PCB are shown in Figure 2.

III. MEASUREMENTS

With the dip probe setup, we have direct control over many operational parameters. These include the setting the first-stage SQUID voltage bias, operating in open loop or flux-locked loop, turning on different numbers of channels of SQUIDs simultaneously, and varying the bias flux applied to the SQUID loop. The focus of this work is measuring changes in SQUID damping of the input resonator while varying the applied bias flux and the number of active channels of the first-stage SQUID chip. For all measurement configurations, eight channels of the second-stage SQUID are used in order to provide a high impedance necessary to drive the output cabling to room temperature.

Figure 3 shows the first-stage SQUID current response to an flux applied by driving a current through the feedback coil. The second-stage SQUID is operated in FLL mode via its feedback coil so that the response of the first-stage SQUID is measured directly. A slowly ramping current is applied to the first-stage SQUID feedback coil, which injects a flux into the SQUID loop. The SQUID response is measured as a function of this current. The response is periodic in Φ_0, so we extract the feedback-SQUID loop coupling of $70\mu\text{A}/\Phi_0$. Figure 3 also demonstrates that multiple SQUID channels can be turned on simultaneously in series with a common voltage bias without distorting the current response, demonstrating that the individual SQUID channels are in phase with each other and adding constructively. Dephasing between channels, which can occur if a SQUID channel has trapped flux or abnormal input coupling, would appear as distortion to the SQUID response curve. The response of the SQUID to small flux perturbations coupled into the input coil from the signal of interest is determined by the slope of the SQUID response at the selected value of bias flux. Changing the bias flux operating point also impacts the SQUID damping.

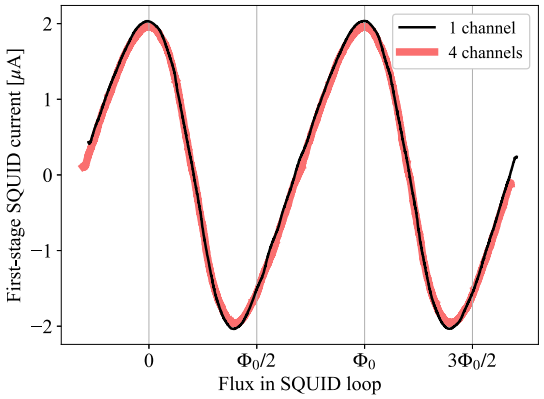

Fig. 3. First-stage SQUID current response to applied bias flux, with bias voltage held constant. Turning on multiple channels adds the SQUID channel responses in phase without causing distortion to the response.

To create a resonator, capacitance is added across the SQUID input. In the following measurements, two capacitors are used. The first capacitor consists of two sheets of Niobium foil separated by a teflon sheet, rolled around a teflon rod for mounting. Niobium leads are spot welded to the capacitor, and connected to the screw terminals. This capacitor has a value of $10.9\pm$ nF measured at 4K. The second capacitor consists of two NPO surface mount capacitors in parallel to produce an increased total capacitance of 20.5 ± 0.3 nF measured at 4K. Unlike most comercially available SMD capacitors, NPO capacitors maintain their capacitance at cryogenic temperatures [16]. The resonant circuit includes lossy components such as resistive aluminum wirebonds, copper traces, and dielectric loss in the capacitor, resulting in quality factors up to $\sim$150.

To describe the SQUID damping effects, we utilize a simple circuit model: the resonator and SQUID effects are written as an equivalent series RLC resonator where the capacitance C is given by the physical capacitance and the inductance and resistance are replaced by:

$$L_{\text{eff}} = L_{\text{fixed}} + \mathscr{L}_{\text{var}}, \tag{1}$$

$$R_{\text{eff}} = R_{\text{fixed}} + \mathscr{R}_{\text{var}}, \tag{2}$$

where $\mathscr{L}_{\text{var}}$ and $\mathscr{R}_{\text{var}}$ are the changing reactive and resistive components of the SQUID-induced damping and are functions of the operating parameters including number of SQUID channels turned on and applied bias flux. The fixed components R_{fixed} and L_{fixed} are determined from Johnson noise spectra measurements performed with a 0Ω jumper replacing the capacitor across the first-stage SQUID input. The temperature is fixed at 4K because it is submerged in liquid helium, and

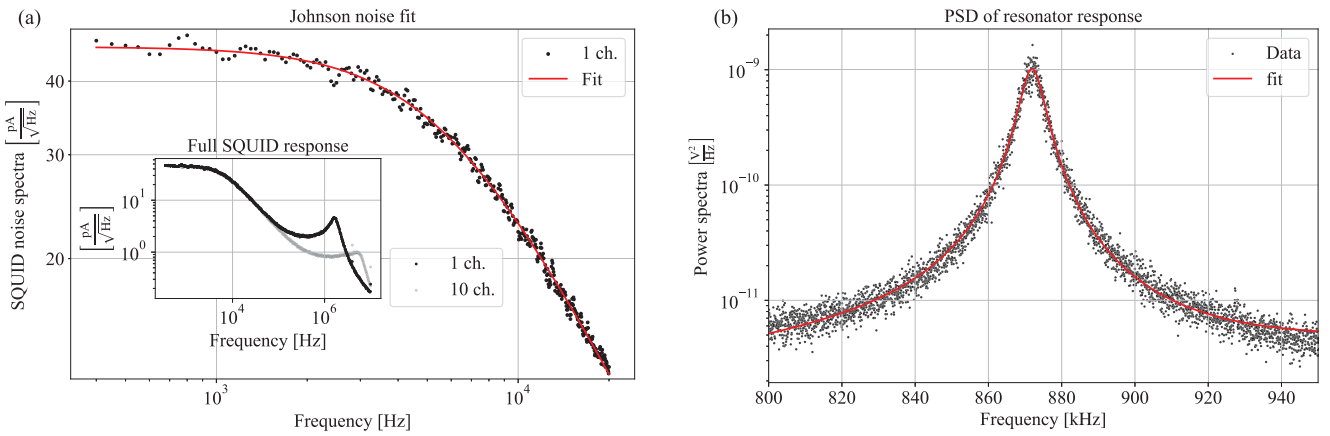

Fig. 4. Noise spectra and fits: (a) To measure the fixed components of the input circuit resistance and inductance, we install a 0Ω jumper across the first stage SQUID input and acquire a Johnson noise spectra of the resulting L/R circuit. The input-referred first stage SQUID current noise in $\mathrm{pA}/\sqrt{\mathrm{Hz}}$ is plotted versus frequency with the fit from Eq. 3 in the 1-channel on configuration. The inset shows the full SQUID response in $\mathrm{pA}/\sqrt{\mathrm{Hz}}$ versus frequency for the 1-channel and 10-channel configurations, operated in FLL mode. While the bandwidth is higher for the 10-channel configuration, the low-frequency L/R pole remains unchanged between configurations. (b) An example noise power spectral density with the niobium-teflon capacitor attached across the first stage SQUID input to form a resonator, measured at the Magnicon output in V^2/Hz. The resonator is centered at 871.97 ± 0.03 kHz and has a quality factor of 129 ± 1. These parameters are extracted using Eq. 4.

we extract the inductance and resistance by measuring the amplitude and 3dB frequency of the noise spectrum:

$$S_{II} = \frac{4k_{\mathrm{B}}T}{R_{\mathrm{fixed}}}\left(1 + \frac{fL_{\mathrm{fixed}}}{2\pi R_{\mathrm{fixed}}}\right)^{-2}. \tag{3}$$

A typical noise spectrum and fit is shown in Figure 4a. Measured values of $L_{\mathrm{fixed}} = 3.06 \pm 0.03\mu\mathrm{H}$ and $R_{\mathrm{fixed}} = 112 \pm 1\mathrm{m}\Omega$ are independent of the number of SQUID channels on. The reactive component L_{fixed} is consistent with the geometric inductance expected from the 10 first-stage SQUID channels (each contributing $\sim 300\mathrm{nH}$) that are wirebonded in.

Figure 4b shows a noise spectra with the niobium and teflon capacitor installed across the first-stage SQUID input. We fit a skewed Lorentzian to the power spectral density in the frequency range of interest. At the resonator frequency the SQUID gain is relatively flat and is accounted for with the skew terms in the fitting function:

$$A(f) = A_1 + A_2\,(f - f_{\mathrm{res}}) + \frac{A_3 + A4(f - f_{\mathrm{res}})}{1 + 4(Q(f - f_{\mathrm{res}})/f_{\mathrm{res}})^2} \tag{4}$$

The A_1 term accounts for white noise background, the terms A_2 and A_4 account for asymmetry in the SQUID gain response. The amplitude of the peak is set by A_3 and the resonator frequency and quality factor are f_{res} and Q respectively.

With this setup, another way to extract the resonator parameters for a given SQUID operating point is to perform a ringdown measurement. In a ringdown measurement, the injection network is used to excite the resonator by applying a near-resonant pulse. After the injection signal has been turned off, the resonator parameters are extracted from the free decay. In order to achieve better signal to noise ratio in ringdowns, the digitized time series of individual ringdown pulses are stacked and averaged before a software lock-in is used to extract the amplitude and phase of the ringdown signal. From the amplitude we extract the resonator decay constant, τ, from an exponential fit with a noise floor:

$$A(t) = A_0 e^{t/\tau} + A_{\mathrm{floor}}, \tag{5}$$

where A_0 is the initial amplitude and A_{floor} is the noise floor. The slope of a linear fit to the phase data gives us the detuning between the resonator frequency and the chosen lock-in frequency which consequenctly gives us f_{res}. Combining τ and f_{res}, we extract the quality factor:

$$Q = \frac{2\pi f_{\mathrm{res}}}{\tau}. \tag{6}$$

We also use the injection network to perform a transfer function measurement of the resonator by measuring the response as the signal on the injection network is swept over the resonator frequency. Transfer functions are a useful tool to investigate non-Lorentzian behaviour of the resonator, and measurements agreed between this method and both the noise spectra and ringdown methods.

From the resonator frequency and capacitance we extract the total inductance L_{eff}:

$$L_{\mathrm{eff}} = \frac{1}{(2\pi f_{\mathrm{res}})^2\, C}. \tag{7}$$

Then, we use L_{eff} and the resonator quality factor to extract R_{eff}:

$$R_{\mathrm{eff}} = \frac{1}{Q}\sqrt{\frac{L_{\mathrm{eff}}}{C}}. \tag{8}$$

For each combination of SQUID channels turned on, we sample at points of applied bias flux in increments of $\sim 70\mathrm{m}\Phi_0$ to finely sample along the full SQUID current response. At each value of flux bias on the first-stage SQUID, we also apply an appropriate dc current to the feedback coil of the second-stage SQUID such that the output to the Magnicon XXF-1 readout is centered at zero. At each operating point, we extract a value

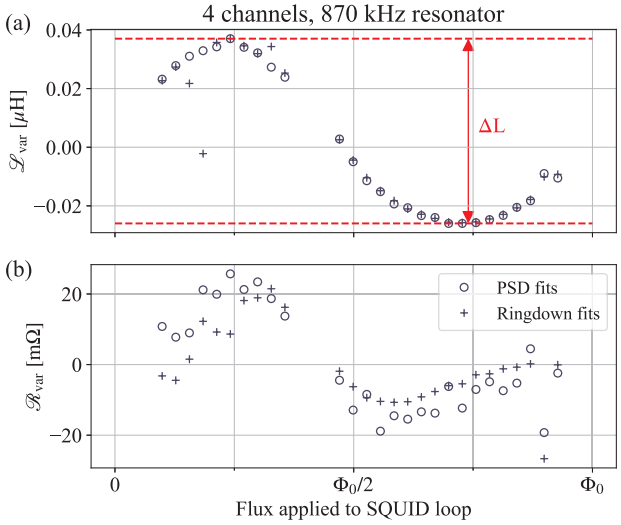

Fig. 5. An example of the varying reactive (a) and resistive (b) components of SQUID damping as a function of applied bias flux with all other operational parameters kept constant. Measurements from ringdowns and noise spectra agree. The data is shown from with 4 channels turned on, and with an 870kHz resonator using the niobium foil and teflon capacitor. Values for the total swing in resistive (ΔR) and reactive components (ΔL) are extracted from this and analogous data sets for other channel combinations and resonator frequencies to produce the results shown in Table II

of $L_{\rm eff}$ and $R_{\rm eff}$ from noise spectra and ringdown measurement techniques described above.

Figure 5 shows how the resistance and inductance of the resonant circuit varies as a function of the applied bias flux for a single resonator frequency and channel combination. Parameters extracted from ringdown and noise spectra fits are in good agreement. Like the SQUID response curve shown in the Figure 3, the values of $\mathscr{R}_{\rm var}$ and $\mathscr{L}_{\rm var}$ are periodic in Φ_0.

TABLE II
EXTRACTED PEAK-TO-PEAK VARIATION IN MEASURED INDUCTIVE AND RESISTIVE COMPONENTS OF SQUID DAMPING

	ΔL	ΔR
870 kHz resonator		
1 channel	14.4 nH	48.9 mΩ
4 channels	63.0 nH	44.9 mΩ
630 kHz resonator		
2 channels	42.9 nH	25.4 mΩ
4 channels	63.1 nH	17.8 mΩ

Values of SQUID damping are dependent on the specific SQUID design, and in this setup the values are measured through the on-chip transformer rather than directly in the SQUID loops. Nonetheless, we can use the above measurements to suggest a range of expected losses from SQUID damping that will inform parameter choices for the next experimental setups. In order to compare dynamic input impedance of different combinations of channels, we extract the peak-to-peak variation in the measured resistive and inductive components, ΔR and ΔL, as shown in Figure 5. Table II shows ΔR and ΔL for different combinations of channels switched on, using resonators at 630 and 870kHz. The inductive contribution approximately scales with the number of channels on, with each channel contributing ∼15nH to ΔL, although there are some discrepancies between measurements at the two different frequencies. In contrast, the variation in the resistive contribution ΔR trends downwards for the 630kHz resonator configuration and trends weakly downwards for the 870kHz resonator configuration as additional SQUID channels are switched on. The small amount of measured loss seen at the input of the transformer decreases as the number of channels switched on increases, which is consistent with low-frequency loss transmission through the transformer.Following the trend described above, we expect that for all 10 channels switched on, ΔR will be smaller than the values in Table II.

IV. APPLICATIONS FOR NEXT-GENERATION EXPERIMENTS

Next steps for these measurements include continuing to probe these SQUID chips and others in this test setup in order to build a comprehensive loss model, with further combinations of operational parameters and resonators. In tandem, we have designed an additional follow-up experiment targeting higher quality factors, to be installed in a dilution refrigerator and with a tunable inductive coupling between the SQUID input and the resonant circuit. This setup will enable measurements of SQUID backaction in addition to damping effects, and will provide additional insight into the desired coupling strength for future experiments including DMRadio. Initially, this follow-up experiment will use the same design of a two-stage TDM dc SQUID arrangement; however, additional SQUID designs may be explored in the future.

The circuit model (up through the first-stage SQUID chip, the follow-on amplification and readout is omitted for simplicity) of this next-stage experiment is shown in Figure 6 (a). The tunable parameter κ changes the coupling between the resonator, with capacitance C, inductance $L_{\rm res}$, and loss $R_{\rm int}$, and a loop that includes the first-stage SQUID chip input coil and the secondary coil of the transformer, $L_{\rm Tr}$. This circuit is written as an equivalent series RLC resonator with effective resistance and inductance, shown in Figure 6 (b). In the regime where the inductive screening term from this second loop is negligible, a SQUID chip with input inductance $L_{\rm SQ}$ and resistive damping contribution $R_{\rm SQ}$ leads to the following effective terms:

$$L_{\rm eff} \approx L_{\rm res}, \tag{9}$$

$$R_{\rm eff} \approx \frac{\kappa^2 R_{\rm SQ} L_{\rm res} L_{\rm Tr}}{\left(L_{\rm SQ} + L_{\rm Tr}\right)^2}, \tag{10}$$

and the quality factor of this resonator is set by both the intrinsic loss in the resonator as well as the SQUID contributions:

$$Q = \left(\frac{1}{Q_{\rm int}} + \frac{1}{Q_{\rm SQ}}\right)^{-1} = \frac{\omega L_{\rm res}}{R_{\rm int} + R_{\rm eff}}. \tag{11}$$

The dilution fridge resonator parameters shown in Table III include conservative SQUID loss estimates from Table II and input inductance for a single first-stage SQUID channel. For this combination of typical parameters, SQUID damping contributions preserve the quality factor above 10^6. In the regime where quality factor degradation from SQUID damping

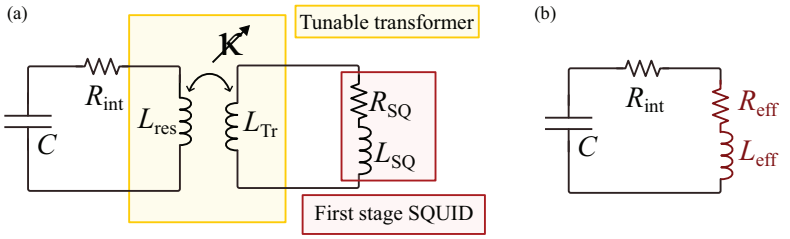

Fig. 6. (a) shows the circuit model of a series RLC resonator coupled via a transformer to the first-stage SQUID chip, which is represented by its damping contributions parameterized as a series resistance R_{SQ} and inductance L_{SQ}. The coupling factor, κ, of the transformer is tunable. We can draw an equivalent series RLC resonator (b) with effective inductance and added resistance given by the Equations 9 and 10. These effective values include the SQUID damping effects reflected through the transformer.

TABLE III
EXAMPLE PARAMETERS FOR FOLLOW-UP HIGH Q RESONATOR

Parameter	**Value**
ω	$2 \times \pi \times 870$kHz
L_{res}	50 µH
L_{Tr}	1 µH
L_{SQ}	300 nH
R_{SQ}	50 mΩ
κ	0.01
Predicted Q_{SQ}	1.8×10^6

is subdominant, a balance between imprecision and backaction noise, set by the coupling between the SQUID and resonator, is optimal for sensitivity in a dark matter experiment [10].

V. CONCLUSION

Using a flexible and reconfigurable SQUID circuit, we have measured the the dynamic input impedance of dc SQUIDs at a two frequencies below 1MHz, probing experimentally relevant SQUID damping effects. This work has established a platform for rapid testing of SQUID chips at multiple operational configurations at 4K in the low-Q, strong coupling regime. Combined with complementary specific test of dc SQUIDs in the high-Q, low-coupling regime at dilution refrigerator temperatures, these test platforms will provide a complete characterization for the selection of SQUIDs and operating parameters for future experiments including DMRadio-m^3, and for characterizing the damping from quantum sensor alternatives to dc SQUIDs.

VI. ACKNOWLEDGMENT

The authors acknowledge the DMRadio collaboration for useful conversations and NIST Boulder for the SQUID chips used in developing the facility. This work was supported by the US Department of Energy, Office of High Energy Physics program under the QuantISED program, FWP 100667.

REFERENCES

[1] C. Hilbert and J. Clarke, "Measurements of the dynamic input impedance of a dc SQUID," *Journal of Low Temperature Physics*, vol. 61, no. 3, pp. 237–262, Nov. 1985. [Online]. Available: https://doi.org/10.1007/BF00681634

[2] S. J. Asztalos *et al.*, "SQUID-Based Microwave Cavity Search for Dark-Matter Axions," *Physical Review Letters*, vol. 104, no. 4, p. 041301, Jan. 2010, publisher: American Physical Society. [Online]. Available: https://link.aps.org/doi/10.1103/PhysRevLett.104.041301

[3] ——, "Design and performance of the ADMX SQUID-based microwave receiver," *Nuclear Instruments and Methods in Physics Research Section A: Accelerators, Spectrometers, Detectors and Associated Equipment*, vol. 656, no. 1, pp. 39–44, Nov. 2011. [Online]. Available: https://www.sciencedirect.com/science/article/pii/S0168900211014483

[4] D. Budker, P. W. Graham, M. Ledbetter, S. Rajendran, and A. O. Sushkov, "Proposal for a Cosmic Axion Spin Precession Experiment (CASPEr)," *Physical Review X*, vol. 4, no. 2, p. 021030, May 2014, publisher: American Physical Society. [Online]. Available: https://link.aps.org/doi/10.1103/PhysRevX.4.021030

[5] V. Popov, "SQUID-based Resonant Detection of Axion Dark Matter," *Journal of Experimental and Theoretical Physics*, vol. 122, no. 2, pp. 236–242, Feb. 2016, arXiv:1410.6682 [hep-ph]. [Online]. Available: http://arxiv.org/abs/1410.6682

[6] S. Uchaikin *et al.*, "Development of SQUID Amplifiers for Axion Search Experiments," in *2019 IEEE International Superconductive Electronics Conference (ISEC)*, Jul. 2019, pp. 1–3.

[7] J. L. Ouellet *et al.*, "First Results from ABRACADABRA-10 cm: A Search for Sub-µeV Axion Dark Matter," *Physical Review Letters*, vol. 122, no. 12, p. 121802, Mar. 2019, publisher: American Physical Society. [Online]. Available: https://link.aps.org/doi/10.1103/PhysRevLett.122.121802

[8] A. Phipps *et al.*, "Exclusion Limits on Hidden-Photon Dark Matter Near 2 neV from a Fixed-Frequency Superconducting Lumped-Element Resonator," in *Microwave Cavities and Detectors for Axion Research*, ser. Springer Proceedings in Physics, G. Carosi and G. Rybka, Eds. Cham: Springer International Publishing, 2020, pp. 139–145.

[9] L. Brouwer *et al.*, "DMRadio-m³: A Search for the QCD Axion Below 1 µeV," Jun. 2022, arXiv:2204.13781 [hep-ex, physics:hep-ph, physics:physics]. [Online]. Available: http://arxiv.org/abs/2204.13781

[10] S. Chaudhuri, K. Irwin, P. W. Graham, and J. Mardon, "Optimal Impedance Matching and Quantum Limits of Electromagnetic Axion and Hidden-Photon Dark Matter Searches," May 2021, arXiv:1803.01627 [hep-ph]. [Online]. Available: http://arxiv.org/abs/1803.01627

[11] DMRadio Collaboration *et al.*, "Projected sensitivity of ${\text{DMRadio-m}}^{3}$: A search for the QCD axion below $1\text{ }\text{ }\mathrm{\ensuremath{\mu}}\mathrm{eV}$," *Physical Review D*, vol. 106, no. 10, p. 103008, Nov. 2022, publisher: American Physical Society. [Online]. Available: https://link.aps.org/doi/10.1103/PhysRevD.106.103008

[12] W. Doriese *et al.*, "Developments in Time-Division Multiplexing of X-ray Transition-Edge Sensors," *Journal of low temperature physics*, vol. 184, no. 1-2, pp. 389–395, Jul. 2016. [Online]. Available: https://www.ncbi.nlm.nih.gov/pmc/articles/PMC4912049/

[13] H. Zappe, "Josephson quantum interference computer devices," *IEEE Transactions on Magnetics*, vol. 13, no. 1, pp. 41–47, Jan. 1977, conference Name: IEEE Transactions on Magnetics.

[14] D. Drung, C. Hinnrichs, and H.-J. Barthelmess, "Low-noise ultra-high-speed dc SQUID readout electronics," *Superconductor Science and Technology*, vol. 19, no. 5, pp. S235–S241, Feb. 2006, publisher: IOP Publishing. [Online]. Available: https://doi.org/10.1088/0953-2048/19/5/s15

[15] "Cryoperm | Cryogenic Magnetic Shielding." [Online]. Available: https://www.mushield.com/magnetic-shielding/cryoperm-cryogenic-magnetic-shielding/

[16] F. Teyssandier and D. Prêle, "Commercially Available Capacitors at Cryogenic Temperatures," *Ninth International Workshop on Low Temperature Electronic*, vol. WOLTE9, p. 5, Jun. 2010. [Online]. Available: https://hal.archives-ouvertes.fr/hal-00623399/document